Nucleic Acids Research, 2025, **53**, gkaf241
https://doi.org/10.1093/nar/gkaf241
Nucleic Acid Therapeutics

AOC 1044 induces exon 44 skipping and restores dystrophin protein in preclinical models of Duchenne muscular dystrophy

Usue Etxaniz[1], Isaac Marks[1], Tyler Albin[2], Matthew Diaz[1], Raghav Bhardwaj[3], Aaron Anderson[1], Olecya Tyaglo[1], Tiffany Hoang[1], Maria Azzurra Missinato[1], Kristoffer Svensson[1], Ben Badillo[1], Philip R. Kovach[1], Laura Leung[1], Michael Cochran[1], Hae Won Kwon[1], Md Nur Ahad Shah[4], Rika Maruyama[4], Toshifumi Yokota[4], Venkata R. Doppalapudi[1], Beatrice Darimont[1], Husam S. Younis[1], W. Michael Flanagan[1], Arthur A. Levin[1], Hanhua Huang[1,*], Georgios Karamanlidis[1,*]

[1]Avidity Biosciences, Inc., 10578 Science Drive, Suite 125, San Diego, CA 92121, United States
[2]Seawolf Therapeutics, 9880 Campus Point Drive, Suite 210, San Diego, CA 92121, United States
[3]Broad Institute of MIT and Harvard, 75 Ames Street, Cambridge, MA 02142, United States
[4]Yokota Lab, Department of Medical Genetics, University of Alberta, Edmonton,T6G 2H, Canada

[*]To whom correspondence should be addressed. Email: georgios.karamanlidis@aviditybio.com
Correspondence may also be addressed to Hanhua Huang. Email: hanhua@aviditybio.com

Abstract

Duchenne muscular dystrophy (DMD) is a severe disorder caused by mutations in the dystrophin gene, resulting in loss of functional dystrophin protein in muscle. While phosphorodiamidate morpholino oligomers (PMOs) are promising exon-skipping therapeutics aimed at restoring dystrophin expression, their effectiveness is often limited by poor muscle delivery. We developed AOC 1044, an antibody–oligonucleotide conjugate (AOC) that combines a PMO-targeting exon 44 with an antibody against the transferrin receptor (TfR1), enhancing delivery to muscle tissues for patients with DMD amenable to exon 44 skipping (DMD44). AOC 1044 induces dose-dependent exon 44 skipping and its mouse-active variant elicited dose-dependent dystrophin restoration in skeletal and cardiac muscle in a DMD mouse model. This treatment also reduced muscle damage, as evidenced by decreases in serum creatine kinase and key liver enzymes, suggesting that restored dystrophin is functionally active. In nonhuman primates, single or repeated AOC 1044 doses resulted in dose-dependent increases in PMO concentration and exon 44 skipping across a range of muscle tissues, including the heart. Collectively, these findings highlight AOC 1044 as a promising therapeutic candidate for patients with DMD44, offering improved muscle targeting and meaningful dystrophin restoration, with potential clinical benefits in reducing muscle degeneration.

Graphical abstract

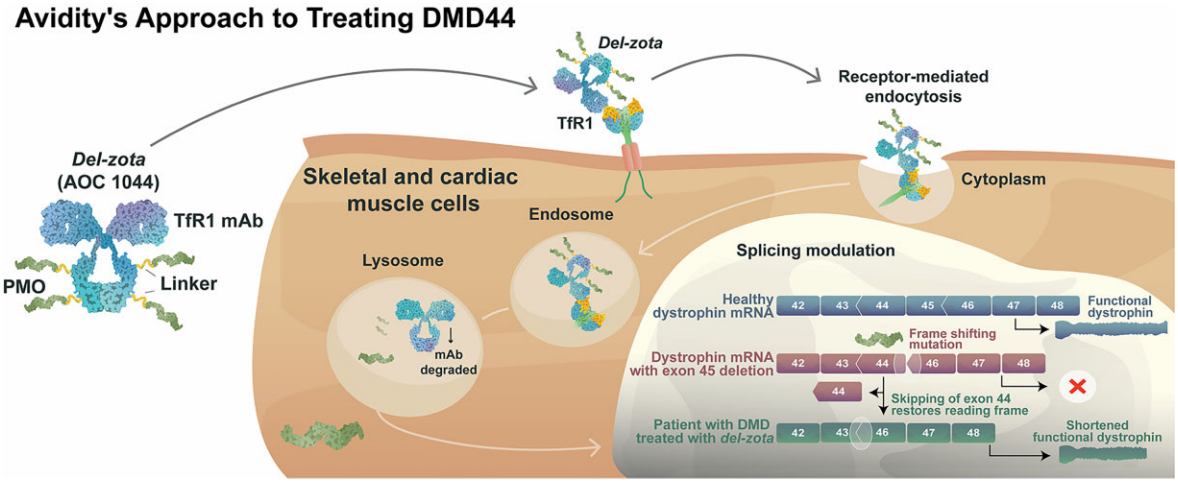

Received: August 7, 2024. **Revised:** March 5, 2025. **Editorial Decision:** March 6, 2025. **Accepted:** March 18, 2025

Introduction

Duchenne muscular dystrophy (DMD) is a severe, life-limiting genetic disorder that affects ∼1 in 5000 newborn boys. This progressive disease is caused by mutations in the dystrophin (*DMD*) gene, which result in little to no production of functional dystrophin protein [1], a critical component responsible for maintaining the strength and stability of muscle fibers. Without dystrophin, muscles such as the heart gradually deteriorate, leading to loss of mobility, heart complications, and premature death [2–4].

The challenge of treating DMD

Dystrophin is essential for linking the muscle's internal structure (cytoskeleton) to its surrounding support system, known as the dystrophin-associated protein complex (DAPC). The absence of dystrophin causes the muscle fibers to weaken over time. A less severe form of the disease, called Becker muscular dystrophy, results from partially functional or truncated dystrophin, suggesting that restoring even some dystrophin could offer meaningful benefits for patients with DMD [5–7].

Since many cases of DMD arise from mutations that disrupt the reading frame of the dystrophin gene, exon-skipping therapies, which "skip" faulty sections of the gene during protein production, have shown promise in restoring the production of a shortened but functional version of dystrophin [8–11]. However, current therapies have limitations. Only four FDA-approved phosphorodiamidate morpholino oligomer (PMO) drugs target patients with DMD who are eligible for exon 45, 51, and 53 skipping [12–15]. Even with these treatments, dystrophin levels remain low—typically below 1% of what is found in healthy muscles [16, 17].

The delivery problem: a barrier to success

A key challenge for PMO therapies is effectively delivering them to muscle tissue, including the heart. Several approaches, such as viral vectors, lipid nanoparticles, and cell-penetrating peptides, have been explored to boost delivery [18–20], and some are currently being tested in the clinic, however PMOs utilizing targeted delivery have yet to be approved. Renal safety concerns have been identified for some cell-penetrating peptides, with development of Sarepta's SRP-5051 peptide-conjugated PMO recently discontinued due to hypomagnesemia (https://www.sarepta.com/community-letter-update-srp-5051-program). This delivery bottleneck limits the effectiveness of current PMO therapies, especially in addressing cardiac symptoms [21–24].

AOC 1044: A new approach with promise

To overcome these delivery challenges, we have developed AOC 1044, an innovative drug that uses antibody–oligonucleotide conjugate (AOC) technology [25, 26]. AOC 1044 combines PMO44, a molecule targeting exon 44 of the dystrophin gene, with a monoclonal antibody (mAb) directed at the transferrin receptor 1 (TfR1). TfR1 is abundant on muscle cells, making it an ideal gateway for targeted drug delivery.

Why AOC 1044 matters for patients with DMD

Around 6% of patients with DMD are eligible for exon 44 skipping, but no disease-modifying therapy has been approved for this group [27]. AOC 1044 offers a potential breakthrough by efficiently delivering PMO44 to skeletal muscle and the heart, where it promotes exon skipping and restores dystrophin production. In this preclinical study, AOC 1044 demonstrated, (i) robust delivery of PMO44 to key tissues, including the heart; (ii) dose-dependent exon 44 skipping and dystrophin expression; and (iii) reduced muscle damage, evidenced by lowered creatine kinase (CK) and liver enzymes [aspartate transaminase (AST) and alanine transaminase (ALT)].

The ability of AOC 1044 to restore dystrophin in both skeletal and cardiac muscle shows great potential to improve outcomes for patients. This novel platform has the potential to address the unmet needs of patients amendable to DMD44 skipping, offering a new potential treatment for improving muscle function and overall quality of life for these patients.

Materials and methods

In vitro experiments

Primary human skeletal muscle cells were obtained commercially (Gibco, #A11440) and were differentiated into myotubes on collagen Type 1 coated 24-well plates (Gibco, #1970788) in Dulbecco's modified Eagle medium (DMEM) supplemented with 2% horse serum (HS) and 1× ITS (Gibco, #1 933 286) according to the manufacturer's instructions for 2 days prior transfection. The Biobank of Cells, tissues, and DNA from patients with neuromuscular diseases, member of the Telethon Network of Genetic Biobanks (project no. GTB12001), funded by Telethon Italy, and of the EuroBioBank network, provided us with specimens (primary myoblasts from DMD patients). Immortalized myoblasts derived from patients with DMD harboring deletion of exon 45 of the dystrophin gene were obtained from the Association Institut de Myologie – Centre de Recherche en Myologie (Sorbonne Université, France). Wild-type (WT) myoblasts derived from healthy muscle were obtained from the Association Institut de Myologie, the University of Rochester (Rochester, NY, USA) and the Centre de Ressources Biologiques (CRB)-Hospices Civils de Lyon (HCL) (Lyon, France) (Supplementary Table S1). Immortalized myoblasts [28] were grown in skeletal muscle growth medium (GM) (Promocell) with gentamicin (Gibco). Primary DMD cells were grown in GM composed of DMEM with Glutamax (Gibco), supplemented with 20% fetal bovine serum (Nucleus Biologics), 10 μg/ml insulin (Sigma), 25 ng/ml human fibroblast growth factor (hFGF) (Stemcell Technologies), 10 ng/ml epidermal growth factor (Stemcell Technologies), and penicillin and streptomycin (Thermo Fisher Scientific). Prior to seeding, 24-well tissue culture plates (Costar) were coated with 1% Matrigel. At ∼80%–90% confluence, myogenic differentiation was induced by replacing GM with differentiation medium (DM): DMEM with Glutamax supplemented with Skeletal Muscle Cell Differentiation Medium Supplement Mix (Promocell). All cell culture experiments were performed with PMO44 for evaluation of exon 44 skipping, dystrophin production, or DAPC activity. To facilitate the PMO uptake by cells, Endo-Porter (1–2 μM, GeneTools, #EP6P1-1) was used.

RNA isolation

Myotubes were collected in Trizol and stored at −80°C until processing for RNA isolation. Frozen tissue samples from mice and monkeys were homogenized in cold Trizol using a TissueLyser II (Qiagen) and Bead Mill Homogenizer (OMNI International), respectively. Total RNA was isolated from cell

lysates or tissue homogenates using Direct-zol-96 RNA isolation kit (Zymo) according to the manufacturer's instructions and quantified with Nanodrop 8000 Spectrophotometer (Thermo Fisher Scientific).

Exon-skipping analysis

A total of 100–500 ng of purified RNA was converted to complementary DNA (cDNA) using a High-Capacity cDNA Reverse Transcription Kit (Applied Biosystems) and a SimpliAmp Thermal Cycler (Applied Biosystems). For quantification by quantitative polymerase chain reaction (qPCR), reactions were cycled 40 times and amplification of total and exon 44-skipped PCR products monitored using QuantStudio 6 or 7 Flex Real-Time PCR instruments (Applied Biosystems). Data were analyzed by QuantStudio™ Real-Time PCR Software v1.3 (Applied Biosystems). The % Exon 44-skipped messenger RNA (mRNA) was calculated as $100^{2} - [CT(skipped) - CT(total)]$. For quantification by droplet digital PCR (ddPCR), cDNA was partitioned into droplets, in triplicate, in the QX200 Automated Droplet Generator (Bio-Rad) in combination with Taqman assays (Thermo Fisher Scientific), 2× ddPCR Supermix for Probes (no dUTP) (Bio-Rad), and BamHI restriction enzyme (New England Biolabs). Following droplet generation, the mixture was loaded into a deep-well C1000 Touch Thermal Cycler (Bio-Rad) for PCR amplification. Absolute quantification of the target RNA molecules was measured in the QX200 Droplet Reader (Bio-Rad) using the QX Manager software (Bio-Rad) [29, 30]. Taqman assays are listed in Supplementary Table S2.

Immunocytochemistry and image analysis by high-resolution microscopy for dystrophin quantification

Quantitative analysis of dystrophin restoration and DAPC assessment in DMD patient-derived cells has been previously described [31]. In brief, human myoblasts from patients with DMD (AB1323, 47811, 47989) were expanded in GM (Zenbio). At day 0, 15 000 human primary myoblasts were seeded per well in GM in 96-well MyoScreen® plates (CYTOO) coated with 10 μg/ml fibronectin (Invitrogen). Induction of differentiation was performed after 24 h of culture by changing the culture medium into DM composed of DMEM:Nutrient Mixture F12 (DMEM/F12; Invitrogen), 2% HS (GE Healthcare), 100 U/ml penicillin, and 100 μg/ml streptomycin (Invitrogen). At day 3, PMO compounds were added to the DMD myotubes and maintained until day 8 post-differentiation. For PMO treatment, PMOs were heated for 5 min at 70°C, then cooled down slowly before addition to the medium. In this specific condition, EndoPorter (GeneTools) was added simultaneously to the wells at 1 μM as delivery reagent. For each experiment, a mock condition corresponding to vehicle ± EndoPorter was included to be used as negative control. At day 9 of culture in MyoScreen® [31], myotubes were fixed with formalin and permeabilized for 15 min with 0.5% Triton in phosphate-buffered saline (PBS). For immunofluorescence staining and dystrophin quantification, cells were blocked with 1% bovine serum albumin, then incubated 2 h at room temperature with primary antibodies prepared in blocking solution: myotubes were stained with a troponin-T specific antibody (ab45932, Abcam, 1:400 dilution) or a myosin heavy chain (MHC)-specific antibody (14-6503-82, Thermo Fisher Scientific, 1:1000). N-Terminal dystrophin was stained using NCL-DysB antibody (Leica, 1:50). Cells were incubated for 2 h at room temperature with the corresponding secondary antibodies in combination with Hoechst 33 342 (Thermo Fisher Scientific, 1:10 000). Images of cells were acquired with the Operetta HCS platform (Perkin Elmer) using a 10× objective, with 11 fields acquired per well. Image processing and analysis were performed using dedicated algorithms developed on the Acapella High Content Imaging Software (Perkin Elmer) by CYTOO. Myotube and nuclei segmentation was performed using the troponin-T or MHC staining intensity and the Hoechst staining. The segmentation threshold was selected to avoid the detection of background noise and eliminate aberrant structures, and myotube area and dystrophin mean intensity were calculated. Four healthy donors were included in each experiment (immortalized AB1167 and three primary myoblast cells: W018, X819, AA179). The mean intensity of dystrophin expression in these healthy myotubes was used as a reference.

Cell profiling for DAPC restoration analysis

For DAPC detection, utrophin (NCL-DRP2, Leica, 1:50 dilution) and alpha-sarcoglycan (ab189254, Abcam, 1:5000) antibodies were used. Based on myotubes segmentation described above, ∼500 features, such as texture and intensity-related categories, were extracted for each myotube DAPCs in fluorescent channels using CellProfiler. A machine learning model was then built to separate the healthy and DMD populations and evaluate efficacy of compounds at restoring a healthy-like phenotype.

Animal treatment and tissue collection

All *in vivo* animal studies were conducted following protocols approved by local Institutional Animal Care and Use Committee (IACUC), in accordance with the regulations outlined in the USDA Animal Welfare Act as well as the "Guide for the Care and Use of Laboratory Animals" [32].

Mouse studies using the humanized DMD mouse model (hDMD^{del45}/*mdx*) were conducted at the University of Alberta in collaboration with Dr Toshifumi Yokota. This DMD mouse model expressing the human dystrophin gene with deletion of exon 45 [33] was kindly provided by Dr Melissa Spencer (UCLA) and crossed to the *mdx* mice obtained from The Jackson Laboratory (B6Ros.Cg-Dmd$^{mdx\text{-}4Cv}$/J, JAX Stock# 002 378). hDMD^{del45}/*mdx* or WT (C57BL/6J) male animals aged 4–6 months were administered a single intravenous (IV) bolus injection of mouse-active antibody–oligonucleotide conjugate (mAOC) 1044 (10, 30 mg/kg), unconjugated PMO44 (30 mg/kg), or respective vehicle. Animals were euthanized at the indicated time points post-dose for collection of serum and muscle tissue. Serum was processed for markers of muscle damage (ALT, AST, CK) using a chemistry analyzer (Beckman Coulter DxC) according to the manufacturer's protocol. Tissue necropsy samples (gastrocnemius, diaphragm, and heart) were collected in 96-well collection microtubes containing a stainless-steel bead and cryobags, snap-frozen, and processed for evaluation of PMO44 concentration, exon 44 skipping, and dystrophin protein as described.

Humanized DMD transgenic mice [Tg(DMD)72Thoen/J] with the full-length human dystrophin gene [34]were acquired from The Jackson Laboratory (JAX Stock# 018 900) and studies were conducted in Explora Biolabs. Male mice,

aged 8–10 weeks, were administered a single dose of either PBS or mAOC 1044 via IV bolus injection in the tail vein at 5 ml/kg body weight. Animals were euthanized at indicated time points. Tissue necropsy samples (gastrocnemius, diaphragm, and heart) were snap-frozen and processed for evaluation of exon 44 skipping.

Studies in C57BL/10ScSn-Dmd*mdx*/J (JAX Stock# 0018) mice were performed in 8–10-week-old males with C57BL/10ScSnJ for control groups and were conducted at The Jackson Laboratories and Explora BioLabs. Mice were dosed either vehicle or mAOC 23 (30 mg/kg) once by a single IV bolus injection in the tail vein at 5 ml/kg body weight. Animals were subjected to muscle function analysis 4 weeks post-dose and euthanized for collection of serum and muscle tissue. For immunofluorescence analysis, whole quadricep muscles were dissected, weight recorded, embedded in optimal cutting temperature compound, and snap-frozen in isopentane and liquid nitrogen. Additional tissue necropsy samples (gastrocnemius, diaphragm, and heart) were snap-frozen and processed for evaluation of exon 23 skipping and dystrophin protein.

Cynomolgus monkey studies were conducted in accordance with the FDA Good Laboratory Practice Regulations, 21 Code of Federal Regulations Part 58 at an AAALAC-accredited contract research laboratory (Altasciences Preclinical Seattle LLC, Everett, Washington). Forty-nine male cynomolgus monkeys (*Macaca fascicularis*, of Cambodian origin; ∼1.8–2.4 years old) were randomly assigned to control and treatment groups. AOC 1044 or vehicle PBS was administered by IV infusion at 10 ml/kg over 60 min using a temporary catheter inserted into a peripheral vein connected to a primed infusion line. Body weights ranged from 1.4 to 1.9 kg at the initiation of dosing. At necropsy, tissue samples were collected in tubes (Omni Hard Tissue Homogenizing Mix, 2-ml reinforced tubes, nuclease, and microbial DNA free Part #19-628D), flash-frozen in liquid nitrogen, and analyzed for PMO44 concentration and exon 44 skipping.

The characterization and description of all AOCs mentioned in the manuscript is listed in Supplementary Tables S3 and S4.

AOC synthesis and purification

AOCs were synthesized as detailed in Cochran *et al.* [26]. PMO oligonucleotides were synthesized by WuXi (Shanghai, China), Genetools (Philomath, Oregon), or Ajinomoto (Tokyo, Japan). The thiol-reactive linker, 4(N-maleimidomethyl)cyclohexanecarboxylic acid N-hydroxysuccinimide ester (SMCC), was coupled to a primary amine on the 3′ end of the PMO by incubating the PMO (50 mg/ml) in phosphate buffer (50 mM phosphate, pH 7.2) with three equivalents of SMCC (50 mg/ml) in dimethyl sulfoxide for 1 h. Excess unconjugated SMCC was removed by tangential flow filtration (TFF) with a membrane molecular weight cutoff (MWCO) of 3 kDa with acetate buffer (10 mM sodium acetate, pH 6.0). AOCs were synthesized by reduction of the interchain disulfide bonds of the antibody with 2 or 2.3 equivalents of Tris(2-carboxyethyl)phosphine hydrochloride for 2 h at 37°C for human immunoglobulin G1 (IgG1) and mouse IgG2c mAb, respectively, prior to incubation with 4.75 equivalents of the maleimide-PMO for 1 h at room temperature. Ten equivalents of ethylmaleimide (NEM) were added to the reaction mixture at room temperature for 30 min to quench unreacted cysteines. Excess PMO and NEM were removed from the AOC reaction mixture using strong cation chromatography purification with GE SP/HP 16 10 resin using a 25 mM acetate, 25 mM Phosphate Buffer (PB), pH 6 buffer ramping up to 25 mM acetate, 25 mM PB, 0.5 mM NaCl, pH 6. The combined fractions were buffer exchanged via TFF (MWCO 70 kDa) into histidine buffer (20 mM histidine, 120 mM sucrose, 10 mM methionine, pH 6) and concentrated to ∼25 mg Ab/ml. The solution was sterile filtered with a 0.22-μm membrane and analyzed by hydrophobic interaction chromatography [average drug-to-antibody ratio (DAR) = 4.0], size exclusion chromatography (3.3% high molecular weight), and a Limulus amebocyte lysate assay (<0.025 EU/mg anti-transferrin receptor antibody) and the product was stored at 4°C. Characterization data are shown in Supplementary Figs S1–S3 and Supplementary Tables S3 and S4.

Muscle function analysis

To evaluate muscle function in by open field test, mice were acclimated to the arena for three consecutive days. Baseline spontaneous activity was monitored for 15 min, then mice were subjected to fatigue challenge for 10 min by hindlimb suspension, which was followed by monitoring of open field spontaneous activity for another 15 min. Distance traveled after the fatigue challenge was quantified (VersaMax, Omnitech Electronics, and Ethovision XT, Noldus).

PMO quantification in tissue samples

Tissue samples were homogenized in Pierce radioimmunoprecipitation assay (RIPA) buffer (Thermo Fisher Scientific) on the TissueLyser II (Qiagen). Sample homogenates were digested with Proteinase K (Promega) to remove the antibody from the PMO. The methodology for the fluorescent enzyme-linked immunosorbent assay (ELISA) for PMO quantification and the DNA probe design have been described previously [35]. Briefly, sample supernatants were diluted appropriately in RIPA dilution buffer, and standard curves containing mPMO23 or hPMO44 were generated in pooled supernatant from PBS-treated control groups to the same final concentration. After the hybridization step of PMO to a complementary DNA probe (Eurofins, IDT) modified with a 3′-biotin and a 5′-digoxigenin, probe-PMO hybrids were added to blocked NeutrAvidin-coated plates and incubated with Micrococcal Nuclease (MNase, Thermo Fisher Scientific), which preferentially cleaves single-stranded DNA. Resulting probe-PMO hybrids were incubated with a monoclonal anti-digoxigenin antibody conjugated with an alkaline phosphatase enzyme before AttoPhos AP Fluorescent Substrate System (Promega) was added to convert the clear substrate into a fluorescent solution. The fluorescence intensity of standards and experimental samples was read on the Tecan Spark (Tecan). Log transformed and parametric regression was performed on standards using a 5PL curve fit in GraphPad Prism, and PMO concentrations of unknown experimental samples were then interpolated within the range of quantitation established of each standard curve. These ELISA assays were method transferred over to an electrochemiluminescence assay on the Meso Scale Discovery Platform for increased sensitivity and precision. This resulted in change to the anti-digoxigenin detection antibody to be conjugated with ruthenium sulfo-Tag and replacement with streptavidin-coated plates.

Dystrophin quantification by Jess Western System

For protein extraction, gastrocnemius, diaphragm, and heart tissue samples were mechanically homogenized in RIPA buffer (Thermo Fisher Scientific) supplemented with Pierce Protease Inhibitor Mini Tablets (Thermo Fisher Scientific) using the Micro-Tube homogenizer (Wilmad-Labglass). The suspension was then centrifuged at 14 000 × *g* for 15 min at 4°C, and glycerol (20% of final volume) was added to the supernatant for cryoprotection. Protein concentrations were measured using the Pierce BCA Protein assay kit (Thermo Fisher Scientific) according to the manufacturer's instructions. Samples were normalized and Jess analysis was performed on a Jess system (ProteinSimple) according to the manufacturer's instructions using a 66- to 440-kDa Separation Module (ProteinSimple), Anti-Rabbit Detection Module, and the Replex Module (ProteinSimple). A rabbit monoclonal anti-dystrophin antibody was used (Abcam ab154168) and diluted 1:1000 in Antibody Dilution Buffer 2 (ProteinSimple). Using Compass software, the resulting electropherograms were inspected to check whether automatic peak detection required any manual correction, and peaks were quantified by calculation of the area under the curve (AUC). The following criteria were used to discriminate low dystrophin signals from background: the peak signal-to-noise ratio given by the software ≥10, and the peak height/baseline ratio ≥3 (protocol adapted from [36]).

To quantify dystrophin levels, a total protein detection module (DM-TP01, ProteinSimple) was used to correct for differences in sample loading or protein content. WT samples were diluted to 15%–20% (*mdx* spiked) to remain in the linear range of detection for both dystrophin and total protein (Supplementary Table S5). Dystrophin restoration was calculated as a percent of the averaged WT group: X animal AUC/(WT AUC average) × 100.

Immunofluorescence of muscle sections

Briefly, frozen muscles were cryosectioned in transverse orientation (5 µm) and collected on positively charged Super Frost slides to maximize tissue adherence. Nonspecific antibody binding was blocked using Novolink Protein Block (Leica) for 30 min. Sections were incubated overnight at 4°C with a mouse anti-Dystrophin antibody (Thermo Fisher Scientific, D8168, 1:50). After washing, a cocktail of secondary antibodies was applied for 60 min at room temperature. Secondary antibodies used were the following: goat anti-rat IgG (H + L) Alexa Fluor Plus 546 (Invitrogen) and goat anti-mouse IgG (H + L) Alexa Fluor Plus 647 (Invitrogen). 4',6-diamidino-2-phenylindole (DAPI) nuclear counterstain was applied. A negative control without primary antibody was included. Samples were scanned as digital whole slide images with the same exposure times.

Pharmacokinetic/pharmacodynamic modeling

A tissue pharmacokinetic (PK)/pharmacodynamic (PD) model relating tissue total PMO to exon skipping and dystrophin levels was developed for gastrocnemius by Certara Strategic Consulting (Montreal, Quebec, Canada). A one-compartment tissue PK model was assumed for total PMO in respective tissues. The increasing total PMO levels were related to increased exon skipping according to indirect response model. A turnover model related increased skipped exon levels to dystrophin levels.

Statistical analysis

GraphPad Prism software was used for all descriptive and statistical analyses. As appropriate, one- or two-way analysis of variance (ANOVA) or *t*-tests were performed for the datasets analyzed. In the case of ANOVA, an appropriate *post-hoc* test was used to determine the differences among the treatment groups. Significant differences were defined as $P < .05$ (two-sided).

Results

PMO44 Activity in DMD-patient-derived myotubes

PMO antisense oligonucleotides have demonstrated the ability to mediate exon skipping and dystrophin production in patients with DMD, so this chemical class was selected as the modality for inducing exon skipping [12–15]. To identify the lead PMO for exon 44 skipping, we conducted a small-scale screening of several sequences proximal to the 5′ end of exon 44. Screening of oligonucleotides was based on evaluation of predicted and experimental data that identified a specific region most proximal to the exon 44 acceptor site on *DMD* mRNA to be most favorable for exon 44 skipping [37]. PMO44 was identified as the lead PMO sequence with an EC_{50} of ∼1 µM for skipping exon 44 (Fig. 1A). In DMD-patient-derived myotubes harboring an exon 45 deletion mutation (DMD^{del45}) that are amenable to exon 44 skipping, PMO44 produced a concentration-dependent increase in the number of exon-44-skipped *DMD* transcripts by up to ∼15-fold compared with untreated cells (Fig. 1B). Notably, there was also an increase in total *DMD* mRNA transcripts with PMO44 treatment compared with vehicle (Fig. 1C), indicating that exon 44 skipping resulted in the formation of mature *DMD* mRNA, although the increase did not reach statistical significance. Low levels of exon 44 skipping may also occur spontaneously in patients [38–41], which is why we can also detect some exon 44 skipping in the vehicle-treated group.

To evaluate whether the skipped exon 44 was able to increase functional dystrophin expression, we employed immunofluorescence assays to measure dystrophin protein as well as formation of DAPCs, which is characteristic of healthier myotubes (Utrophin and Alpha Sarcoglycan stained to evaluate DAPCs). Treatment with PMO44 increased dystrophin protein in a concentration-dependent manner in DMD^{del45} myotubes (Fig. 2A-B). The production of dystrophin protein was present in most myotubes, indicating that PMO44 was active uniformly in myotubes. DAPC formation requires the presence of dystrophin protein to stabilize the complex for the contraction and relaxation of myofibers [42–44]. PMO44 treatment produced a concentration-dependent restoration of DAPC in DMD^{del45} myotubes (Fig. 2C). This finding provides evidence that truncated dystrophin protein resulting from skipping exon 44 restores towards a healthy-like phenotype *in vitro*. It is worth noting that these results were obtained from myotubes derived from patients with DMD who had an exon 45 deletion (DMD^{del45}), which represents the most common disease-causing mutation amenable to exon 44 skipping [40, 45].

mAOC 1044 is pharmacologically active in a humanized mouse model of DMD ($hDMD^{del45}$/*mdx*)

To evaluate the *in vivo* pharmacological activity of PMO44, we leveraged a transgenic mouse model of DMD that

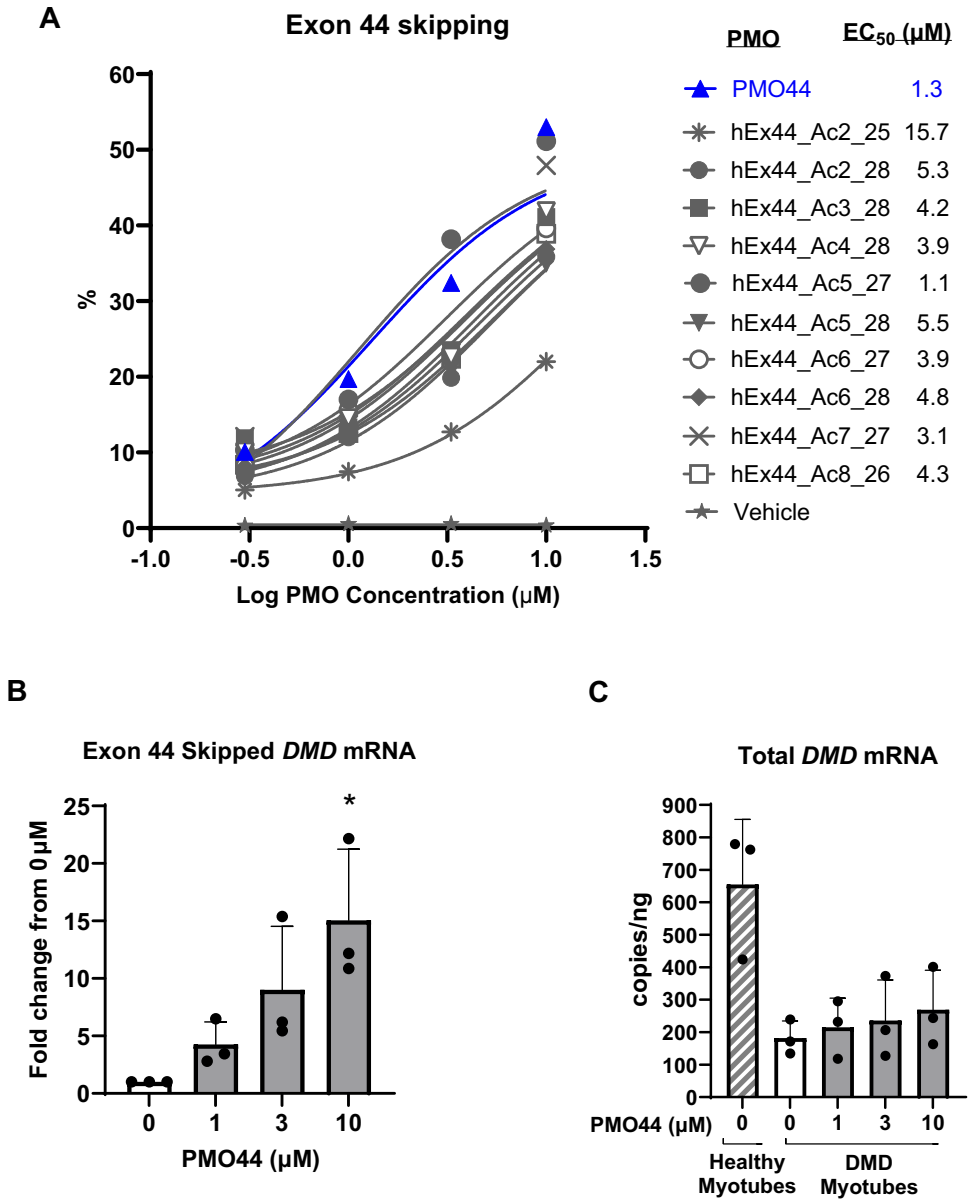

Figure 1. PMO44-mediated exon 44 skipping in DMD-patient-derived myotubes. (**A**) Primary human skeletal myotubes were treated with PMOs (0.3–10 μM) using Endoporter as a transfection reagent. Total and exon 44-skipped *DMD* mRNA transcripts were quantified by reverse-transcription quantitative polymerase chain reaction (RT-qPCR) at 48 h post-treatment. Data represent means from a single experiment performed in duplicate. (**B**, **C**) Myotubes derived from myoblast cell lines from DMD patients were treated with PMO44 (0–10 μM). Healthy myotubes were also included as a control in (**C**). Exon-44-skipped mRNA and total *DMD* (exon 73–74) levels were determined by ddPCR 48 h post-treatment. Data are presented as mean ± standard error of the mean (SEM), $n = 3$/group. * Statistical difference relative to vehicle control ($P < .05$) using one-way ANOVA with Dunnett's *post-hoc* test.

expresses the human dystrophin gene harboring an exon 45 deletion in the *mdx* background (hDMD^{del45}/*mdx*) [33]. We chose this mouse model because we wanted to eliminate expression of a mouse dystrophin protein (*mdx* background) to simulate exon 44 skipping from the disease allele (hDMD^{del45}), which is more relevant to patients with DMD. It is also worth mentioning that we previously noticed, from various internal cell culture data, that exon 44 skipping varies greatly between a WT and a DMD^{del45} sequence (data not shown). To further probe this observation in a relevant *in vivo* setting and eliminate any bias due to cell culture conditions, we evaluated exon 44 skipping in a mouse model expressing the full-length human WT dystrophin gene and a mouse model expressing the human *DMD^{del45}* gene in the *mdx* background (lacking the mouse dystrophin protein), hDMD^{del45}/*mdx*, which is amenable to exon 44 skipping. Given that the anti-TfR1 antibody component of AOC 1044 does not bind to mouse TfR1, we conjugated PMO44 to an anti-mouse TfR1 antibody and generated a mouse-active molecule (mAOC 1044) to enable TfR1-mediated delivery to muscles (Fig. 3A). As hypothesized, exon 44 skipping was significantly greater in all muscles tested in the hDMD^{del45}/*mdx* model compared to the WT DMD humanized mouse model (Fig. 3B and C). This data suggests the increase in exon 44 skipping in the disease genotype is not due to differences in PMO tissue uptake but rather to a more permissive skipping

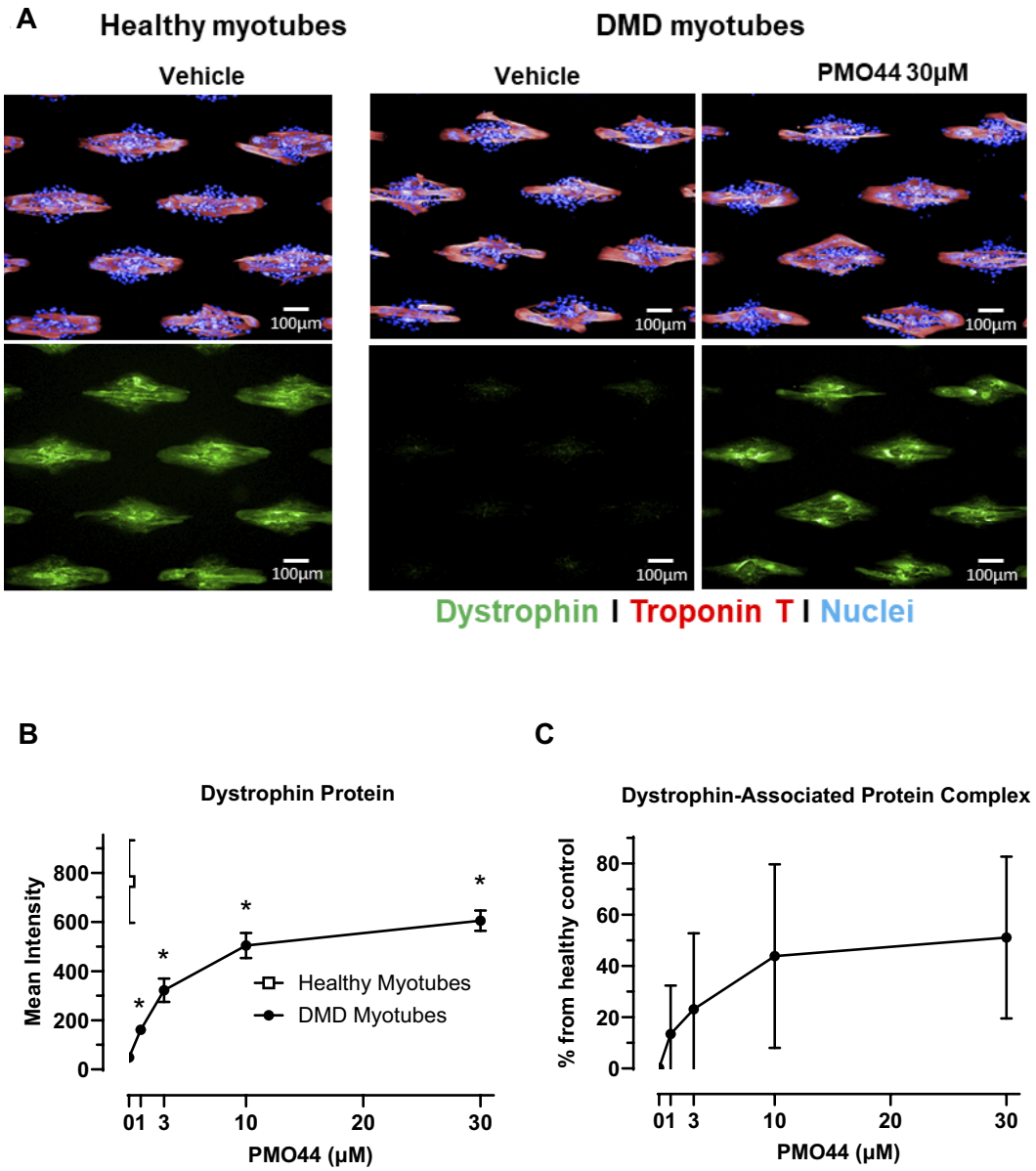

Figure 2. PMO44-mediated dystrophin protein restoration in DMD-patient-derived myotubes. (**A**) Dystrophin protein (green staining) was evaluated by immunofluorescence after 6 days of PMO treatment. (**B**) Quantitative microscopy of dystrophin staining was performed after 6 days of PMO treatment. (**C**) DAPC was evaluated after 6 days of PMO treatment using quantitative immunofluorescence using CellProfiler to evaluate restoration. Data were acquired using Operetta HCS imaging system and analyzed using Acapella software (PerkinElmer) and are plotted as means ± SEM. DMD myotubes were derived from three different patients, and $n = 4$ for healthy myotubes, >50 myotubes per replicate were analyzed. *$P < .05$ relative to 0 μM using one-way ANOVA with Dunnett's *post-hoc* test.

environment. As such, this model is more appropriate for simulating skipping in human patients with DMD44.

To further characterize mAOC 1044, we treated hDMD^{del45}/*mdx* at two different doses (10 or 30 mg/kg per PMO component) with mAOC 1044 and compared it to unconjugated PMO44 (30 mg/kg). We also harvested muscle tissues after 2 and 4 weeks to better characterize the drug pharmacokinetic properties. As expected, a single dose of unconjugated PMO44 (30 mg/kg) had no detectable PMO44 in muscle tissues. Treatment with unconjugated PMOs typically requires more frequent treatments at higher doses to achieve any meaningful activity. In contrast, a single dose of mAOC 1044 (10 or 30 mg/kg, PMO44 component) produced dose-dependent PMO44 concentrations in skeletal muscle (gastrocnemius and diaphragm) and heart tissue that remained relatively elevated even at 4 weeks post-dosing in both the 10 and 30 mg/kg dose groups (Fig. 4A–C). It has been previously shown that higher overall TfR1 expression in skeletal muscle tissue may partly explain the observed tissue selectivity [25, 46, 47]. Commensurate with the delivery of PMO44 in muscle tissue, dose-dependent exon 44 skipping was observed at both the 10 and 30 mg/kg dose groups. The extent of exon 44 skipping ranged from 3- to 25-fold above that in vehicle-treated animals across skeletal and cardiac muscles and was maintained for at least 4 weeks post-dose (Fig. 4D–F). More importantly, mAOC 1044

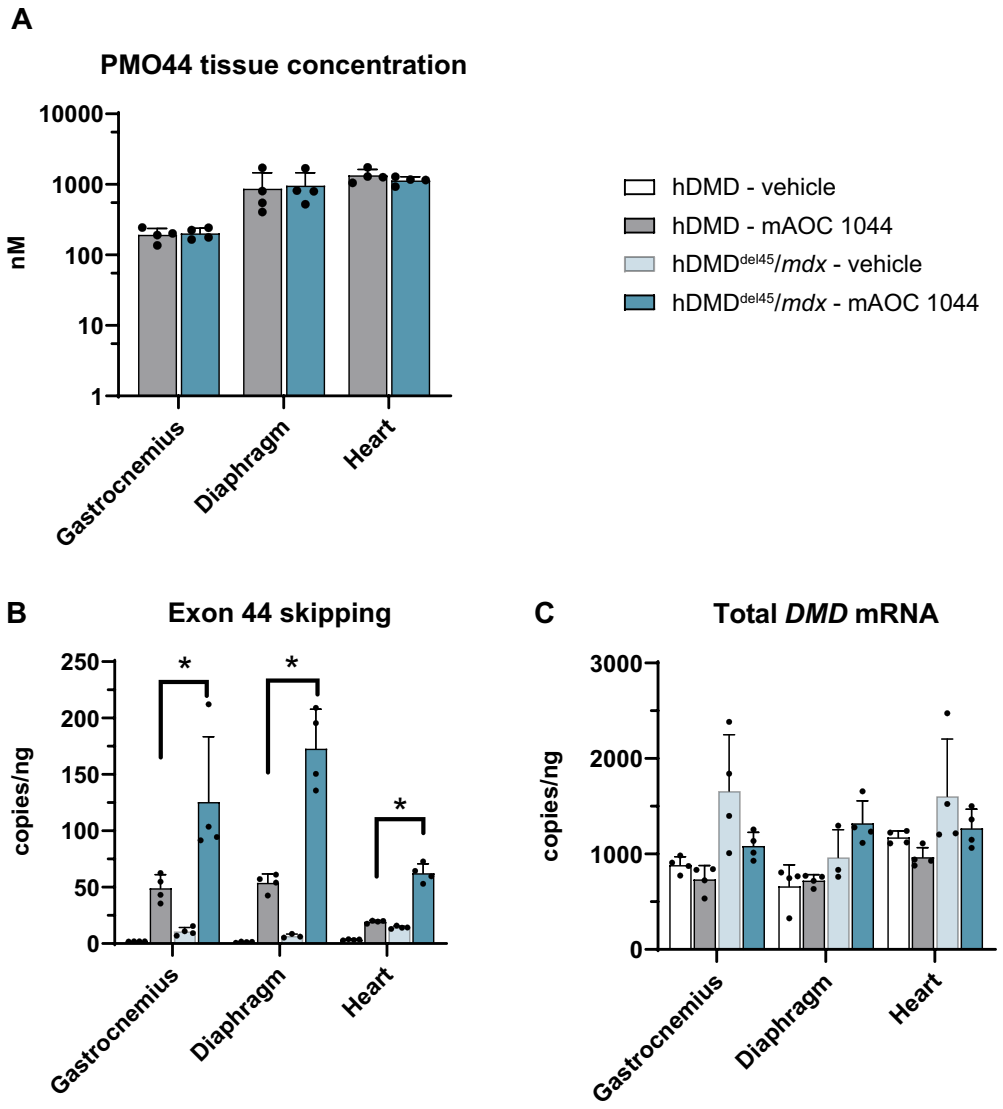

Figure 3. mAOC 1044 exon 44 skipping in mice expressing WT hDMD or hDMD^{del45}/*mdx*. (**A**) PMO44 concentration, (**B**) exon 44 skipping, and (**C**) total *DMD* mRNA in mice administered a single IV dose of mAOC 1044 (30 mg/kg, per PMO44 component) from which muscle tissue was harvested at 2 weeks post-dose. Data presented as mean ± SEM, $n = 3$–4 per group. $^*P < .05$ compared to WT, using unpaired *t*-test.

produced marked increases in dystrophin protein levels in muscle tissue at 10 and 30 mg/kg. The extent of dystrophin protein production increased from 2 to 4 weeks of treatment in all muscle tissue evaluated (Fig. 4G–I). This increase is likely due to the lag in protein synthesis and accumulation. Four weeks after a single dose, mAOC 1044 at 30 mg/kg produced 10%, 11%, and 6% of dystrophin in gastrocnemius, diaphragm, and heart, respectively. Vehicle-treated hDMD^{del45}/*mdx* had <1% dystrophin in these tissues and it was undetectable in most animals.

Unconjugated PMO44 failed to increase exon 44 skipping or dystrophin production relative to vehicle-treated animals, confirming the tissue delivery limitations of unconjugated PMOs. In contrast, mAOC 1044 data highlight the effectiveness of the AOC platform to deliver substantial concentrations of PMO44 to skeletal and heart muscle tissue that are pharmacologically active. Of note there is a sharper drop in exon 44 skipping in the diaphragm at 30 mg/kg group (Fig. 4E). However, this does not seem to be the case for the group dosed at 10 mg/kg.

A model was developed based on results obtained from gastrocnemius muscle of hDMD^{del45}/*mdx* mice that describes the relationship of PMO44 concentration with exon skipping and dystrophin production. The dashed lines represent a model simulation of the change as a function of PMO44 concentration in gastrocnemius muscle (as a representative skeletal muscle tissue) of exon skipping (blue line) and dystrophin protein as a % of WT (black line) overlayed with the observed hDMD data. PMO44 muscle concentrations above 20 nM are sufficient to produce increases in exon 44 skipping and dystrophin protein (Fig. 5).

mAOC 1044 reduced serum biomarkers of muscle damage in a humanized mouse model of DMD (hDMD^{del45}/*mdx*)

We next wanted to evaluate whether restoration of dystrophin protein expression in the hDMD^{del45}/*mdx* mouse model can improve biomarkers including CK, ALT, and AST, which are often used in the clinical setting to evaluate muscle tissue damage. Indeed, treatment with mAOC 1044 not only im-

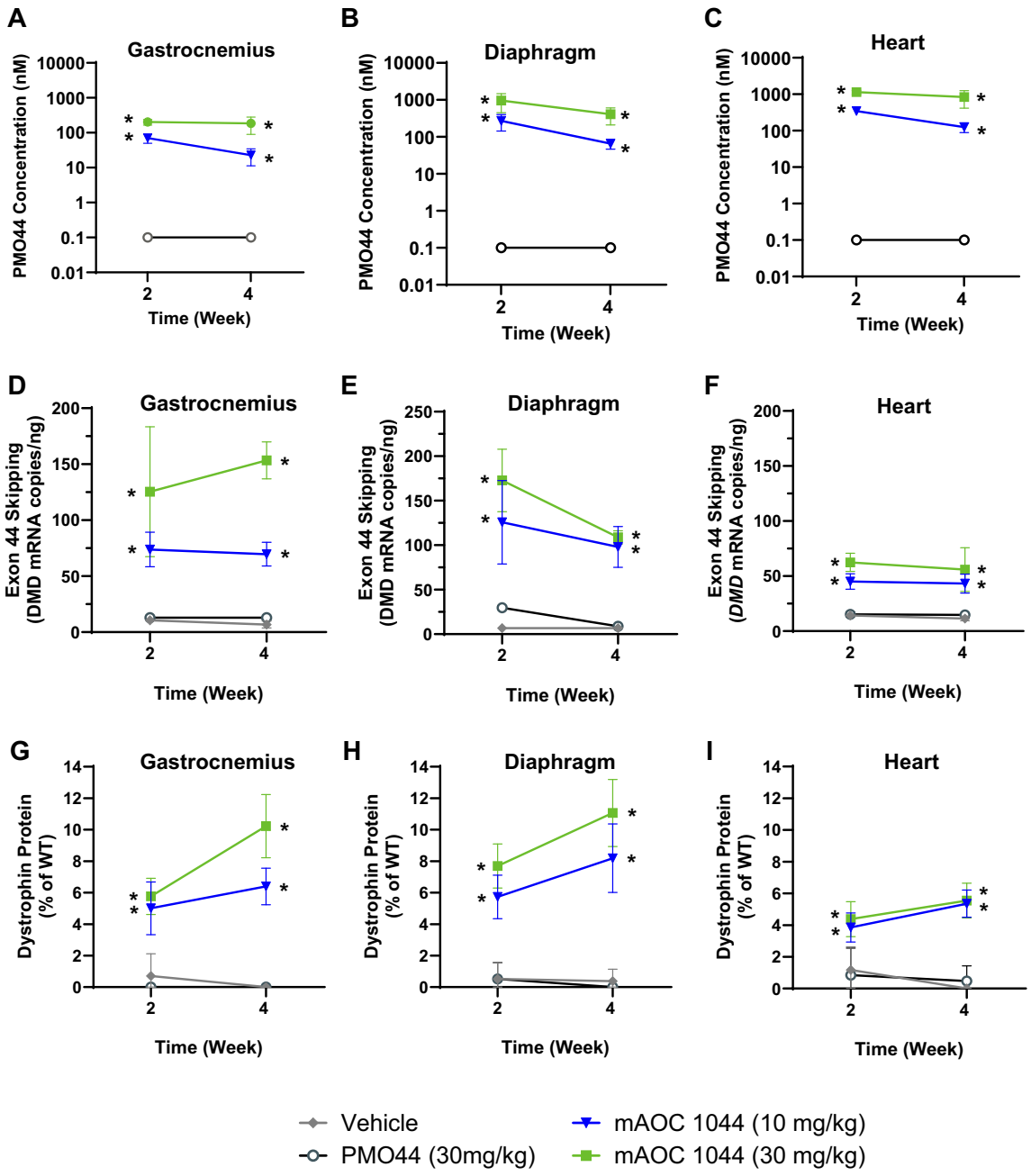

Figure 4. mAOC 1044 produced increased PMO44 muscle tissue concentration in hDMD^{del45}/*mdx* mice. hDMD^{del45}/*mdx* mice were administered a single IV dose of mAOC 1044 (10 or 30 mg/kg, per PMO44 component) or unconjugated PMO44 (30 mg/kg) and muscle tissue was collected 2 or 4 weeks after dosing ($n = 4$/group). (**A**–**C**) PMO concentrations, (**D**–**F**) exon-44-skipped *DMD* mRNA, and (**G**–**I**) dystrophin protein was evaluated in gastrocnemius, diaphragm, and heart muscles. All PMO44 dose group samples had values below the limit of quantification (5.4 nM). Data presented as mean ± SEM. All mAOC 1044 treatment groups at all time points were statistically significant relative to vehicle control *($P < .05$) using two-way ANOVA with Tukey's *post-hoc* test. This figure displays data from an experiment that utilized the same set of animals, $n = 4$ per group.

proved dystrophin protein restoration as shown in Fig. 4 but also generally reduced the levels of these serum biomarkers in a dose-dependent manner (Fig. 6A–C). Given the increased variability in these measurements and the low power of the study, while all the numerical values trended lower in all three biomarkers, only AST in the group treated with mAOC 1044 at 30 mg/kg per PMO equivalent reached statistical significance. Treatment with unconjugated PMO trended to have higher values in all three serum biomarkers, which was unexpected given that PMOs are in general well tolerated *in vivo*. Collectively, these data suggest that mAOC 1044 can effectively deliver PMO44 to skeletal muscle and heart tissue and trigger exon 44 skipping, resulting in production of functional dystrophin protein and decreased muscle damage.

Treatment with mAOC 23 improves muscle function in the *mdx* mouse model of DMD

To further confirm whether the AOC platform can achieve homogeneous dystrophin restoration and restore skeletal muscle function in a different model, we used the well-established *mdx* mouse model of DMD [48], which is amenable to exon

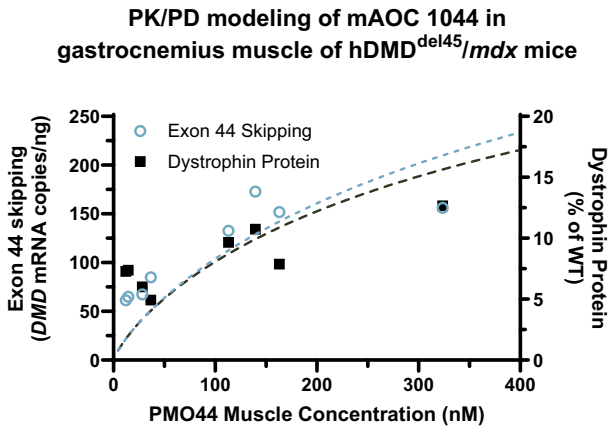

Figure 5. PK/PD profile of mAOC 1044 in gastrocnemius muscle of hDMD^{del45}/*mdx* mice. hDMD^{del45}/*mdx* mice were administered a single IV dose of mAOC 1044 (10 or 30 mg/kg, PMO44 component). The PK/PD model was developed based on the PMO44 concentrations, exon 44 skipping, and dystrophin protein production in muscle at 4 weeks post-dose, $n = 4$/group.

23 skipping. For this model, we developed mAOC 23, an AOC targeting exon 23, designed to restore dystrophin. Following a single dose of 30 mg/kg mAOC 23 (per PMO component), we observed substantial exon 23 skipping and up to ~20% dystrophin restoration in the gastrocnemius muscle (Fig. 7A).

To assess the distribution of dystrophin, sections from the quadriceps muscle were analyzed using immunofluorescence. Muscle cross-sections were stained for dystrophin that align in the sarcolemmal membrane and DAPI to mark nuclei (Fig. 7B). As expected, WT muscle displayed robust dystrophin expression along the sarcolemma, maintaining membrane integrity. In contrast, *mdx*-vehicle-treated muscles exhibited little to no detectable dystrophin, consistent with the muscle degeneration characteristic of DMD. However, muscles from mAOC 23-treated *mdx* mice showed clear dystrophin restoration along the sarcolemmal membrane, mimicking WT-like patterns, confirming the successful delivery of the PMO and efficient exon skipping. Notably, the restored dystrophin was evenly distributed across the evaluated myofibers, underscoring the therapeutic potential of the AOC platform to achieve homogeneous dystrophin restoration.

Given the promising molecular results, we next sought to determine the functional impact of mAOC 23 treatment on muscle performance. To evaluate muscle function, the mice underwent a muscle fatigue challenge followed by an open-field test to monitor their movement and activity. In the open-field assay, WT mice exhibited extensive movement represented by dense red movement tracks, reflecting normal muscle function (Fig. 7C and D). In comparison, vehicle-treated *mdx* mice showed limited movement and sparse tracking, consistent with the profound muscle weakness characteristic of DMD. Importantly, mAOC 23-treated *mdx* mice demonstrated enhanced movement capacity, as evidenced by increased tracking, suggesting functional improvements corresponding with the restored dystrophin expression.

AOC 1044 is pharmacologically active in nonhuman primates

To assess the pharmacological activity and sustained efficacy of the clinical candidate AOC 1044 in higher species, we conducted studies in NHPs (Cynomolgus monkeys), leveraging the cross-reactivity of AOC 1044 with the TfR1 receptor in this species. Nonhuman primates (NHPs) were administered AOC 1044 at different doses (5, 15, or 45 mg/kg PMO44) via IV infusion every 4 weeks for 3 months. AOC 1044 treatment resulted in dose-dependent increases in PMO44 concentrations across multiple muscle tissues, including the heart, gastrocnemius, and diaphragm (Fig. 8A). Notably, PMO44 accumulation was consistently higher in cardiac tissue compared to other muscle groups, indicating greater uptake in the heart. These findings align with previous observations in mouse models. Consistent with the presence of PMO44 in muscle, dose-dependent exon 44 skipping was achieved across all tested doses (Fig. 8B). At the highest dose (45 mg/kg), exon 44 skipping levels increased by 90- to 155-fold relative to vehicle-treated animals, demonstrating robust pharmacological engagement of the therapeutic target. In addition, AOC 1044 exhibited pharmacological activity across a wide range of skeletal muscle tissues after a single 30 mg/kg dose (Fig. 8C), underscoring the compound's ability to induce exon skipping across muscle groups.

Together, these results confirm the broad muscle tissue penetration, sustained activity, and target engagement of AOC 1044 in NHPs, supporting its potential as a therapeutic candidate for patients with DMD44. The observed dose-dependent muscle distribution and pronounced cardiac uptake are particularly encouraging for addressing both skeletal and cardiac manifestations of the disease.

AOC 1044 is well-tolerated in NHPs

The AOC platform represents a novel approach for targeted delivery of oligonucleotide therapeutics to muscle tissues. As such, we evaluated the safety and tolerability of repeated administration of AOC 1044 in NHPs given that AOC 1044 is pharmacologically active in NHPs. AOC 1044 was well tolerated at IV doses up to 45 mg/kg, administered every four weeks for nine months. No significant changes were observed in body weight (Fig. 9A), and electrocardiogram parameters such as heart rate, PR interval, and QRS interval remained within normal limits throughout the study (Fig. 9B–D). Additionally, no treatment-related adverse effects were identified across a range of safety assessments, including clinical observations, safety pharmacology parameters (e.g. respiratory rate, blood gas, body temperature, neurobehavioral assessments), immune function, ophthalmology, clinical pathology, organ weights, and macroscopic and microscopic evaluations of a full panel of tissues (data not shown).

Treatment-related effects included alterations in serum iron levels and unsaturated iron-binding capacity, consistent with transient modulation of TfR1 activity. These iron-related changes were associated with mild, dose-dependent differences in red blood cell parameters that were generally minimal, transient, and reversed during or after the nondosing phase (Supplementary Table S6). Additionally, minimal to mild basophilic granules containing PMO oligonucleotides were detected in specific tissues, including the renal tubular epithelium and Kupffer cells in the liver, across all tested doses. At the highest dose (45 mg/kg), basophilic granules

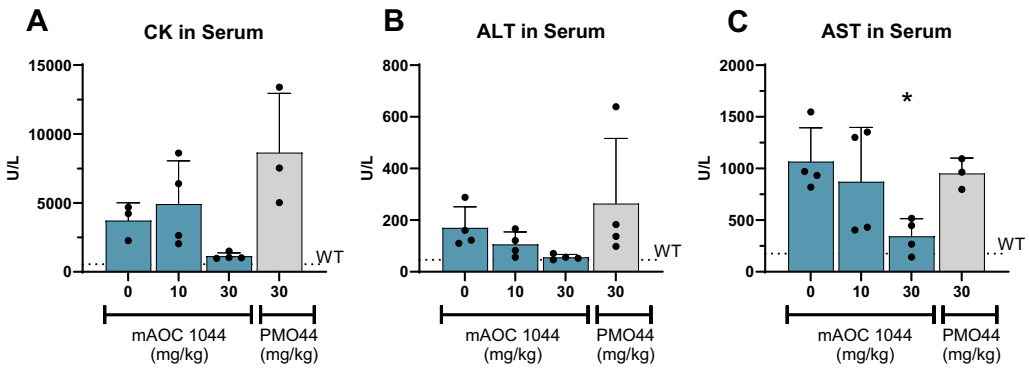

Figure 6. mAOC 1044 produced reductions in serum markers of muscle damage in hDMD^{del45}/*mdx* mice (4–6 months old). (**A**) CK (**B**) ALT and (**C**) AST in serum collected from hDMD^{del45}/*mdx* mice treated with a single IV dose of mAOC 1044 (0, 10, or 30 mg/kg, PMO44 component) or unconjugated PMO44 (30 mg/kg) for 4 weeks. Data presented as mean ± SEM, $n = 4$/group. *$P < .05$ relative to 0 mg/kg group using one-way ANOVA with Dunnett's *post-hoc* test. The data shown in this figure were obtained from the same set of animals shown in Fig. 4, collected at 4 weeks post-dose.

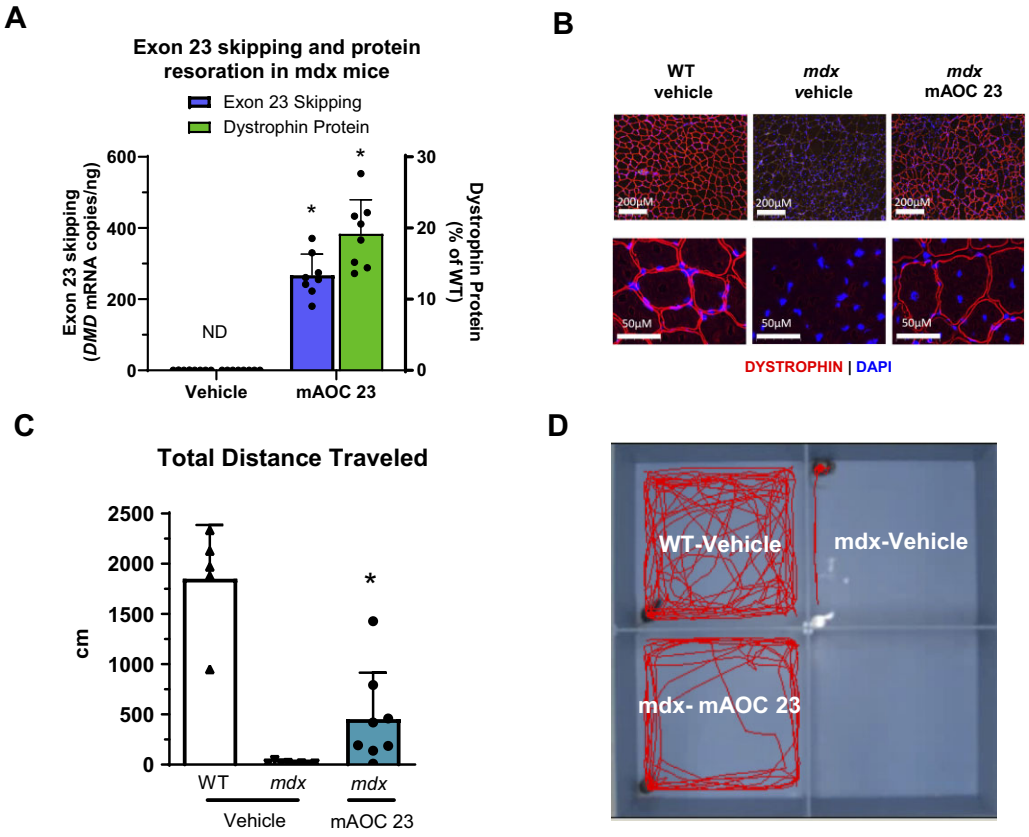

Figure 7. Pharmacological and functional activity of mAOC 23 in the *mdx* mouse model of DMD. *Mdx* mice were administered a single IV dose of vehicle or mAOC 23 at 30 mg/kg (per PMO23 component). WT animals were administered a single dose of vehicle. (**A**) Exon 23 skipping, and dystrophin protein were evaluated in gastrocnemius tissue 4 weeks after dosing. (**B**) Representative micrograph of dystrophin protein staining in quadriceps muscle. (**C**) Distance traveled in open field arena was quantified. Data are presented as means ± SEM, $n = 4$–8/group, *$P < .05$ compared to *mdx*-vehicle group using an unpaired *t*-test. (**D**) A representative image of the open field arena test for a single mouse in each group is shown for illustration purposes. In this figure, panels (A) and (C)/(D) reflect data from different animal sets within the same experiment, while panel (B) presents data from different animals in an independent study.

were accompanied by mild vacuolation of the renal tubular epithelium (Supplementary Table S7). These observations are consistent with previously reported findings for oligonucleotide therapeutics, including PMOs, and reflect expected uptake and sequestration of oligonucleotides in endolysosomes. Importantly, these changes were considered nonadverse due to their minimal severity, reversibility, and the absence of any functional impairments in the kidney or liver [49, 50].

Discussion

While several exon-skipping therapeutic approaches for DMD have emerged, their efficacy has been hampered by challenges

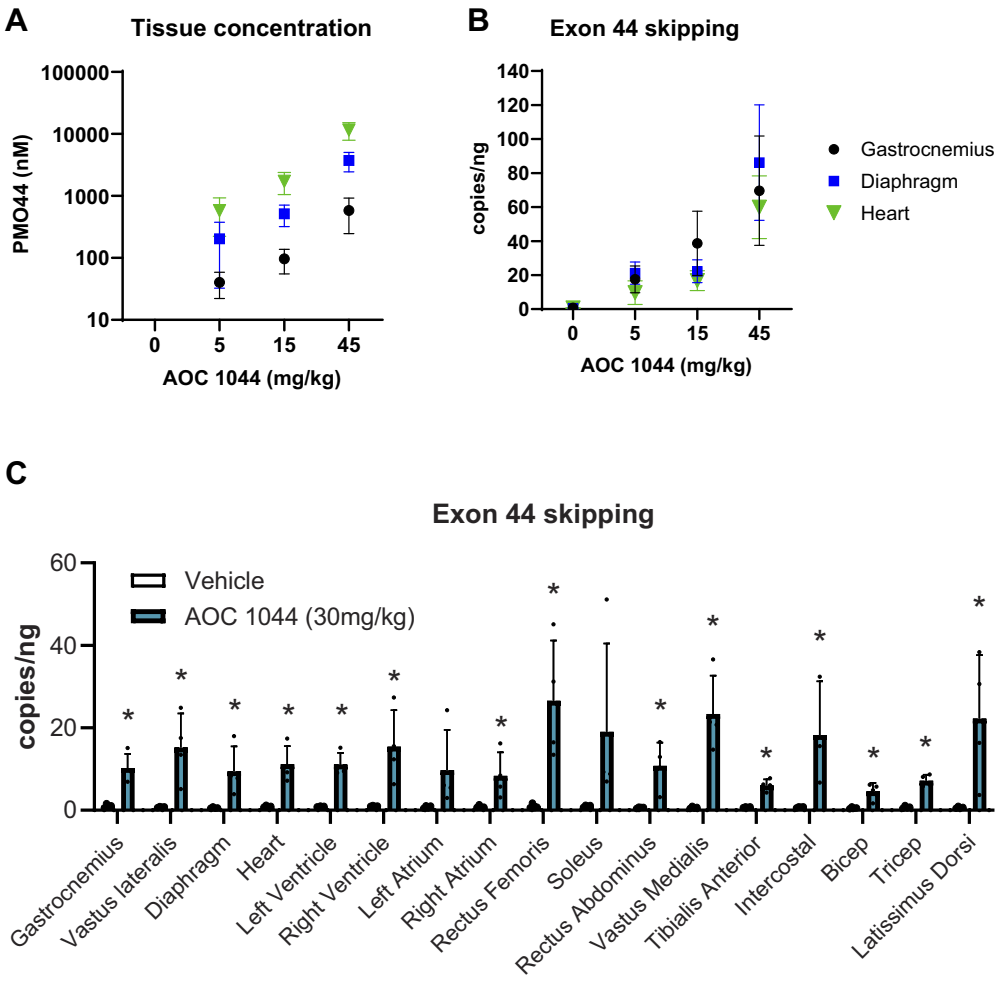

Figure 8. AOC 1044 produced dose-dependent increases in PMO44 concentration and exon 44 skipping in muscle of NHPs. (**A**) PMO44 tissue concentration and (**B**) exon 44 skipping in NHPs administered IV AOC 1044 (0, 5, 15 or 45 mg/kg PMO44 component) every 4 weeks for 3 months. Data are presented as mean ± SEM, $n = 3$–5/group/time point. (**C**) Exon 44 skipping in a range of skeletal muscles in monkeys 6 weeks after receiving a single injection of AOC 1044 at 30 mg/kg (based on the PMO44 component). Data are presented as mean ± SEM. $^*P < .05$ compared to vehicle group, $n = 4$ group using unpaired *t*-test. In this figure, the same animal set was used for the tissue concentration and exon skipping data. Panel (C) presents data from an independent NHP study.

in effectively delivering oligonucleotides to muscles. We have addressed this challenge by developing the AOC platform that demonstrates highly efficient and productive oligonucleotide delivery in skeletal muscle and the heart tissues [25]. AOC 1044 was developed for treating patients with DMD44 and is designed to specifically target exon 44 in the *DMD* pre-mRNA, using TfR1-mediated delivery to skeletal and cardiac muscle tissue. AOC 1044 produced durable exposure of PMO44 to muscle tissue in a dose-dependent manner in NHPs and in mice. These results are consistent with our previous observations with siRNA oligonucleotide-conjugated AOCs [25] and further substantiate the utility of the TfR1 antibody in facilitating the efficient delivery of oligonucleotides to muscle and heart tissue. Its efficacy in targeting cardiac muscle is important because cardiomyopathy accounts for a considerable proportion of DMD-related mortality [3, 51, 52]. Therefore, delivery of PMO44 to the heart provides potential for increased dystrophin production in this tissue that may improve overall clinical outcomes.

Therapeutic implications and functional benefits of AOC 1044

Our data confirm that PMO-based exon skipping can indeed restore truncated yet functional dystrophin protein, as demonstrated by increased dystrophin levels and the reformation of the DAPC. This is particularly significant, as the reformation of DAPC has been identified as essential for stabilizing the muscle membrane, mitigating muscle damage, and preserving contractile function. Moreover, mAOC 1044 not only restored dystrophin expression in the hDMD^{del45}/mdx mouse model, but also improved muscle health, as evidenced by reduced serum biomarkers of muscle damage (e.g. CK, ALT, and AST). These findings suggest that even partial restoration of dystrophin can yield significant clinical benefits, which is consistent with other preclinical studies showing that even low levels of dystrophin (10%–20% of normal levels) can improve physical performance in functional tests and substantially slow disease progression and in DMD animal models [53, 54]. In particular,

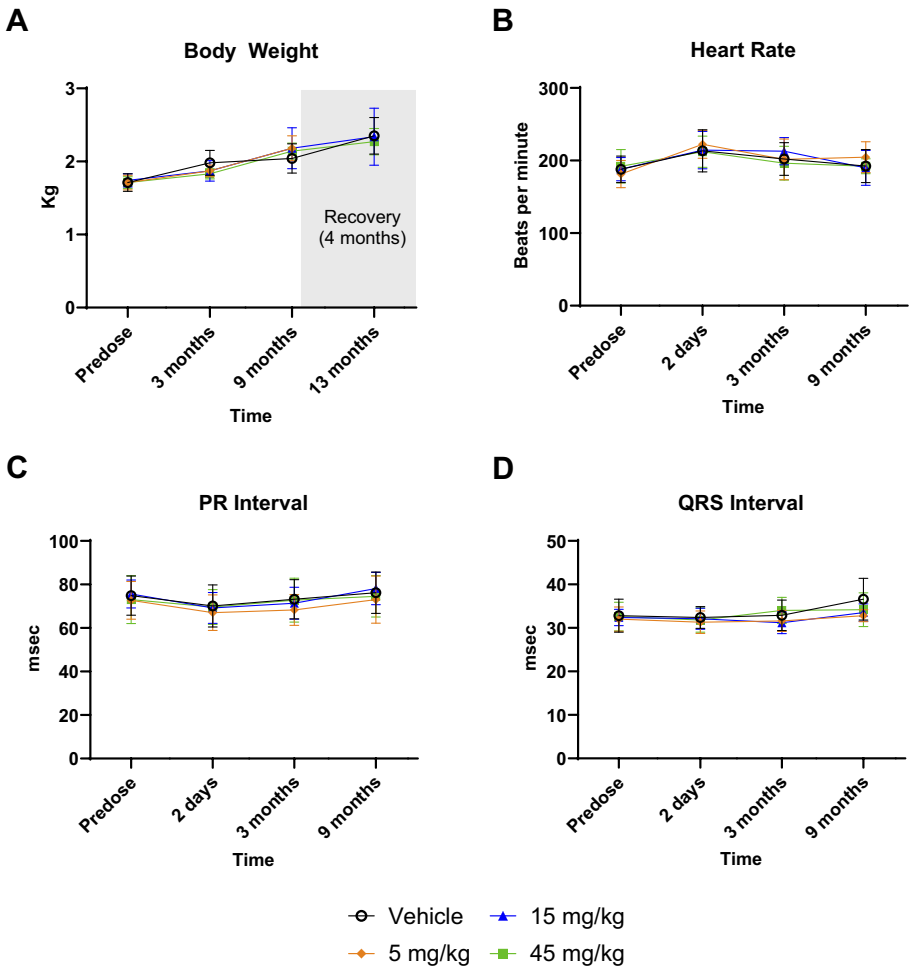

Figure 9. AOC 1044 was well-tolerated in NHPs following 9 months of treatment. (**A**) Body weight (**B**), heart rate (**C**), PR interval (**D**), and QRS interval in NHPs administered IV AOC 1044 (vehicle or 5, 15, or 45 mg/kg PMO44 component) every 4 weeks for up to 9 months, followed by a 4-month treatment-free period wherever indicated. Data are presented as mean ± SD, $n = 3$–13 for body weight and $n = 5$–13 for electrocardiogram. The same animals were analyzed over time.

the marked dystrophin restoration in cardiac tissue observed in our study is noteworthy, given that cardiomyopathy is a major cause of morbidity and mortality in patients with DMD. The increased cardiac uptake of PMO44 following AOC delivery offers the potential to address both skeletal muscle and cardiac manifestations of the disease, which remains a significant challenge in current exon skipping therapies.

Additionally, the results from mAOC 23 treatment in the *mdx* model of DMD demonstrate a uniform distribution of dystrophin along muscle fibers. This suggests that AOC therapy not only restores dystrophin expression but does so in a homogeneous manner across muscle tissues, which is crucial for maintaining muscle integrity and preventing localized areas of weakness. This contrasts with gene therapy-based treatments that often do not show homogeneous dystrophin expression in muscle.

AOC 1044 also exhibited exon 44 skipping in NHPs, a pharmacologically relevant preclinical species. Repeated dosing demonstrated a sustained effect in all muscle tissues that were evaluated, over a prolonged 3-month period. Collectively, these results highlight the broad pharmacological activity of AOC 1044 in both skeletal and cardiac muscles across multiple preclinical species.

Comparison of AOC 1044 with existing exon skipping therapies

Targeting TfR1 for delivering oligonucleotides into cardiac and skeletal muscles has been widely recognized for its therapeutic potential in muscular diseases, as demonstrated by our group and others [25, 26, 53, 55]. Our findings also align with the growing body of research supporting antisense oligonucleotide-mediated exon skipping as a promising therapeutic strategy for DMD [56]. For example, previous clinical trials with eteplirsen targeting exon 51, casimersen targeting exon 45, and golodirsen targeting exon 53 have shown some success in restoring dystrophin production in patients with DMD; however, functional efficacy data have not been successfully produced yet [12, 13, 15]. Unconjugated PMOs, like the currently approved therapies, require multiple doses at relatively high PMO concentrations to enable their detection in tissues and achieve minimal exon skipping (<1%). In contrast, AOC 1044 achieved >1000× higher tissue concentration compared to unconjugated PMOs when dosed at the same PMO level, which substantially increased exon 44 skipping and sustained dystrophin protein restoration for a longer time. This gives AOC 1044 the potential to provide superior efficacy and potentially modify disease progression to a

greater extent compared to unconjugated PMO based therapies, while also reducing dose frequency and making it a more patient-friendly treatment.

This enhanced delivery efficiency and dystrophin protein restoration underscore the advantage of using the AOC platform. AOCs that engage TfR1 expressed in muscle tissues improve the bioavailability and tissue penetration of therapeutic molecules, addressing a key limitation in existing exon skipping strategies.

Comparison of AOC 1044 with alternative delivery strategies

While our AOC technology consists of mAbs, alternative modalities such as antibody fragments (Fabs) have also been explored. An anti-TfR1-Fab with PMO23 also demonstrated improved exon skipping compared with the unconjugated oligonucleotide in *mdx* mice [53]. Notably, differences in study designs and methodologies preclude definitive conclusions or direct comparisons across various technologies. However, there are a few potential benefits using the AOC platform over Fab-based technology. Fab-based delivery vehicles can have faster plasma clearance rates due to their smaller size compared to full-size antibodies, resulting a short half-life in plasma which can reduce the amount of PMO delivered to tissues. Another potential advantage of using full-size antibodies in the AOC platform is the ability to conjugate multiple PMOs per antibody. AOC 1044 has an average DAR of about 4, meaning it has about four PMOs attached to each antibody. Fabs in general have lower DARs, which reduces the amount of PMO that can be delivered.

Other strategies aim to improve *in vivo* delivery and cellular uptake of PMOs through conjugation to peptides, facilitating PMO entry into cells across the cell membrane. These approaches include peptide–PMO conjugates (PPMOs), such as cell-penetrating peptides, PMO internalization peptides, muscle-targeting peptides, and endosomolytic peptides [23, 24, 54, 58]. Unfortunately, direct comparison of published data from different PPMOs in *mdx* mice is not feasible. However, the overall pharmacology data are comparable to the mAOC 23 data shown herein. However, it remains unclear whether renal toxicity associated with high PPMO doses can be mitigated without compromising cardiac delivery and efficacy [21, 24]. In contrast, AOC 1044 was well-tolerated in NHPs for up to 9 months with minimal, treatment-related effects and no signs of toxicity.

In summary, our studies with AOC 1044 in NHPs, a pharmacologically relevant preclinical model, highlight the safety and efficacy profile of the AOC platform.

Challenges in exon-skipping evaluation

Evaluating exon-skipping therapies with precision, sensitivity, and reproducibility remains a challenge. In non-DMD genotypes, exon skipping disrupts the dystrophin gene reading frame rather than restoring it, complicating the evaluation. Other studies have suggested that DMD transcripts with out-of-frame mutations are expected to be unstable and prone to degradation, making accurate measurement more challenging [57].

Here, we chose to present the data as skipped copies to avoid any normalization bias. Using ddPCR, a method that allows precise quantification of transcript levels, we observed lower exon 44 skipping in healthy NHPs compared to the hDMD^{del45}/*mdx* mouse model. We have only shown percent-skipping in Fig. 1A, because in that initial experiment we utilized RT-qPCR before switching to ddPCR for greater precision. Comparative studies with humanized DMD mouse models expressing the full-length WT or mutant dystrophin gene confirmed that exon skipping is more pronounced in models with DMD mutations than in those with the intact WT gene. Hence, the exon 44 skipping data from hDMD^{del45}/*mdx* mice may have a better predictive value for forecasting skipping in human patients with DMD. Data from NHPs may be used to confirm activity and PMO delivery with the clinical candidate AOC 1044 since the TfR1 antibody has similar affinity to the NHP TfR1 receptor.

Clinical development and broader potential

The encouraging preclinical results of AOC 1044 support its potential as a promising treatment for DMD44. Preclinical pharmacokinetics and pharmacodynamics data in DMD mouse models suggested that PMO44 concentrations >20 nM in muscle are sufficient to produce at least 5% increase in dystrophin production. In this regard, allometric scaling of monkey plasma and muscle tissue pharmacokinetics was used to identify doses of AOC 1044 in humans that would achieve at least 20 nM muscle tissue concentrations. AOC 1044 is currently being evaluated in the EXPLORE44 clinical trial for patients with DMD44 (NCT05670730), with positive preliminary data in Phase 1/2 (https://aviditybiosciences.investorroom.com/2024-08-09-Avidity-Biosciences-Announces-Positive-AOC-1044-Data-Demonstrated-Significant-Increase-of-25-in-Dystrophin-Production-and-Reduction-of-Creatine-Kinase-Levels-to-Near-Normal-in-People-Living-with-Duchenne-Muscular-Dystrophy-Amenable-to-Exon-44-S). Beyond DMD, the versatility of AOC therapeutics extends to other muscle diseases. Clinical trials for AOC 1001 and AOC 1020 are ongoing for myotonic dystrophy type 1 (MARINA-OLE; NCT05479981) and facioscapulohumeral muscular dystrophy (FORTITUDE; NCT05747924), respectively.

Conclusion

In summary, AOC 1044 offers significant advantages over traditional PMO therapies and a promising approach for treating DMD44 by achieving enhanced delivery, potent exon skipping, and sustained dystrophin restoration across multiple tissues. The favorable safety profile and pharmacological activity observed in preclinical models, along with ongoing clinical trials, suggest that AOC technology may revolutionize the treatment of muscular diseases through RNA therapeutics. These advancements highlight the potential of AOCs to provide disease-modifying therapies for a broad spectrum of skeletal muscle and cardiac disorders.

Acknowledgements

We thank Yanling Chen, Michael Moon, Mehul Dhanani, and Verna Zhao for assistance with *in vivo* studies; Dr Vincent Mouly (Association Institut de Myologie, Centre de Recherche en Myologie, France) for providing immortalized human myoblast cell lines derived from one apparently healthy donor AB1167C20FL and from one patient with DMD AB1323; the “Biobank of Cells, tissues and

DNA from patients with neuromuscular diseases", member of the Telethon Network of Genetic Biobanks (project no. GTB12001), funded by Telethon Italy, and of the EuroBioBank network, for primary human myoblasts derived from patients with DMD (ID#: 47811 and 47898); Prof. Laurent Schaeffer and Hospices Civils De Lyon (HCL)-CBC BioTec; the University of Rochester and Dr Tawil for providing primary myoblasts from apparently healthy donors; Erwann Ventre, Melanie Flaender and Giulio Morozzi from CYTOO for assistance with dystrophin and DAPC studies *in vitro*; Orsolya Kiraly from the Jackson Laboratory for assistance with the *mdx* mouse model functional study; Vivienne Bunker and Satoru Oneda from Altasciences Preclinical for assistance with the NHP studies; Lauren Todd, PhD, CMPP from Sixsense Strategy Group, Toronto, ON, Canada for editorial support. We sincerely thank Courtney S. Young and Melissa J. Spencer (UCLA) for granting us a license to use the hDMDdel45/mdx mice developed in their laboratory.

Author contributions: Conceptualization and study design: U.E., I.M., T.A., M.D., R.B., K.S., L.L., M.C., T.Y., V.R.D., B.D., H.S.Y., W.M.F., A.A.L., H.H., G.K. Data collection and analysis: U.E., I.M., T.A., M.D., R.B., A.A., O.T., T.H., M.A.M., K.S, B.B., P.R.K., L.L., M.C., H.W.K., M.N.A.S., R.M., T.Y., B.D., G.K. Manuscript writing and review: U.E., I.M., K.S., M.C., V.R.D., H.S.Y., W.M.F., A.A.L., H.H., G.K.

Supplementary data

Supplementary data is available at NAR online.

Conflict of interest

Usue Etxaniz, Isaac Marks, Michael Cochran, and Venkata R. Doppalapudi are employees of Avidity Biosciences, Inc. who receive stock and stock options and have patent applications or pending or awarded patents. Matthew Diaz, Aaron Anderson, Olecya Tyaglo, Tiffany Hoang, Maria Azzurra Missinato, Kristoffer Svensson, Ben Badillo, Philip R. Kovach, Laura Leung, Hae Won Kwon, Husam S. Younis, W. Michael Flanagan, Arthur A. Levin, Hanhua Huang, and Georgios Karamanlidis are employees of Avidity Biosciences, Inc. who receives stock and stock options. Tyler Albin, Raghav Bhardwaj, Maria Azzurra Missinato, and Beatrice Darimont are former employees of Avidity Biosciences, Inc and may hold stock and/or stock options (and Tyler Albin and Beatrice Darimont have patent applications). Toshifumi Yokota and Rika Maruyama are cofounders and shareholders of OligomicsTX, Inc.

Funding

The work was supported by Avidity Biosciences, Inc., San Diego, CA. Editorial support was funded by Avidity Biosciences, Inc. Funding to pay the Open Access publication charges for this article was provided by Avidity Biosciences.

Data availability

All available data have been included in the manuscript. Additional data are available on request from Avidity Biosciences, Inc., San Diego, CA. Supplementary data are available at NAR online.

References

1. Juan-Mateu J, Gonzalez-Quereda L, Rodriguez MJ *et al.* DMD mutations in 576 dystrophinopathy families: a step forward in genotype-phenotype correlations. *PLoS One* 2015;**10**:e0135189. https://doi.org/10.1371/journal.pone.0135189
2. Hoffman EP, Brown RH Jr., Kunkel LM. Dystrophin: the protein product of the Duchenne muscular dystrophy locus. *Cell* 1987;**51**:919–28. https://doi.org/10.1016/0092-8674(87)90579-4
3. Ryder S, Leadley RM, Armstrong N *et al.* The burden, epidemiology, costs and treatment for Duchenne muscular dystrophy: an evidence review. *Orphanet J Rare Dis* 2017;**12**:79. https://doi.org/10.1186/s13023-017-0631-3
4. Duan D, Goemans N, Takeda S *et al.* Duchenne muscular dystrophy. *Nat Rev Dis Primers* 2021;**7**:13. https://doi.org/10.1038/s41572-021-00248-3
5. Findlay AR, Wein N, Kaminoh Y *et al.* Clinical phenotypes as predictors of the outcome of skipping around DMD exon 45. *Ann Neurol* 2015;**77**:668–74. https://doi.org/10.1002/ana.24365
6. Beggs AH, Hoffman EP, Snyder JR *et al.* Exploring the molecular basis for variability among patients with Becker muscular dystrophy: dystrophin gene and protein studies. *Am J Hum Genet* 1991;**49**:54–67.
7. Comi GP, Prelle A, Bresolin N *et al.* Clinical variability in Becker muscular dystrophy. Genetic, biochemical and immunohistochemical correlates. *Brain* 1994;**117**:1–14. https://doi.org/10.1093/brain/117.1.1-a
8. Lu QL, Yokota T, Takeda S *et al.* The status of exon skipping as a therapeutic approach to Duchenne muscular dystrophy. *Mol Ther* 2011;**19**:9–15. https://doi.org/10.1038/mt.2010.219
9. Arechavala-Gomeza V, Anthony K, Morgan J *et al.* Antisense oligonucleotide-mediated exon skipping for Duchenne muscular dystrophy: progress and challenges. *Curr Gene Ther* 2012;**12**:152–60. https://doi.org/10.2174/156652312800840621
10. Niks EH, Aartsma-Rus A. Exon skipping: a first in class strategy for Duchenne muscular dystrophy. *Expert Opin Biol Ther* 2017;**17**:225–36. https://doi.org/10.1080/14712598.2017.1271872
11. Levin AA. Treating disease at the RNA level with oligonucleotides. *N Engl J Med* 2019;**380**:57–70. https://doi.org/10.1056/NEJMra1705346
12. Syed YY. Eteplirsen: first global approval. *Drugs* 2016;**76**:1699–704. https://doi.org/10.1007/s40265-016-0657-1
13. Heo YA. Golodirsen: first approval. *Drugs* 2020;**80**:329–33. https://doi.org/10.1007/s40265-020-01267-2
14. Dhillon S. Viltolarsen: first approval. *Drugs* 2020;**80**:1027–31. https://doi.org/10.1007/s40265-020-01339-3
15. Shirley M. Casimersen: first approval. *Drugs* 2021;**81**:875–9. https://doi.org/10.1007/s40265-021-01512-2
16. Charleston JS, Schnell FJ, Dworzak J *et al.* Eteplirsen treatment for Duchenne muscular dystrophy: exon skipping and dystrophin production. *Neurology* 2018;**90**:e2146–54. https://doi.org/10.1212/WNL.0000000000005680
17. Frank DE, Schnell FJ, Akana C *et al.* Increased dystrophin production with golodirsen in patients with Duchenne muscular dystrophy. *Neurology* 2020;**94**:e2270–82. https://doi.org/10.1212/WNL.0000000000009233
18. Godfrey C, Desviat LR, Smedsrod B *et al.* Delivery is key: lessons learnt from developing splice-switching antisense therapies. *EMBO Mol Med* 2017;**9**:545–57. https://doi.org/10.15252/emmm.201607199
19. Roberts TC, Langer R, Wood MJA. Advances in oligonucleotide drug delivery. *Nat Rev Drug Discov* 2020;**19**:673–94. https://doi.org/10.1038/s41573-020-0075-7
20. Hammond SM, Aartsma-Rus A, Alves S *et al.* Delivery of oligonucleotide-based therapeutics: challenges and opportunities. *EMBO Mol Med* 2021;**13**:e13243. https://doi.org/10.15252/emmm.202013243
21. Amantana A, Moulton HM, Cate ML *et al.* Pharmacokinetics, biodistribution, stability and toxicity of a cell-penetrating

peptide-morpholino oligomer conjugate. *Bioconjug Chem* 2007;**18**:1325–31. https://doi.org/10.1021/bc070060v
22. Moulton HM, Moulton JD. Morpholinos and their peptide conjugates: therapeutic promise and challenge for Duchenne muscular dystrophy. *Biochim Biophys Acta* 2010;**1798**:2296–303. https://doi.org/10.1016/j.bbamem.2010.02.012
23. Gait MJ, Arzumanov AA, McClorey G *et al.* Cell-penetrating peptide conjugates of steric blocking oligonucleotides as therapeutics for neuromuscular diseases from a historical perspective to current prospects of treatment. *Nucleic Acid Ther* 2019;**29**:1–12. https://doi.org/10.1089/nat.2018.0747
24. Tsoumpra MK, Fukumoto S, Matsumoto T *et al.* Peptide-conjugate antisense based splice-correction for Duchenne muscular dystrophy and other neuromuscular diseases. *EBioMedicine* 2019;**45**:630–45. https://doi.org/10.1016/j.ebiom.2019.06.036
25. Malecova B, Burke RS, Cochran M *et al.* Targeted tissue delivery of RNA therapeutics using antibody–oligonucleotide conjugates (AOCs). *Nucleic Acids Res* 2023;**51**:5901–10. https://doi.org/10.1093/nar/gkad415
26. Cochran M, Marks I, Albin T *et al.* Structure-activity relationship of antibody–oligonucleotide conjugates: evaluating bioconjugation strategies for antibody-phosphorodiamidate morpholino oligomer conjugates for drug development. *J Med Chem* 2024;**67**:14868–84. https://doi.org/10.1021/acs.jmedchem.4c00803
27. Bladen CL, Rafferty K, Straub V *et al.* The TREAT-NMD Duchenne muscular dystrophy registries: conception, design, and utilization by industry and academia. *Hum Mutat* 2013;**34**:1449–57. https://doi.org/10.1002/humu.22390
28. Mamchaoui K, Trollet C, Bigot A *et al.* Immortalized pathological human myoblasts: towards a universal tool for the study of neuromuscular disorders. *Skeletal Muscle* 2011;**1**:34. https://doi.org/10.1186/2044-5040-1-34
29. Hiller M, Falzarano MS, Garcia-Jimenez I *et al.* A multicenter comparison of quantification methods for antisense oligonucleotide-induced DMD exon 51 skipping in Duchenne muscular dystrophy cell cultures. *PLoS One* 2018;**13**:e0204485. https://doi.org/10.1371/journal.pone.0204485
30. Verheul RC, van Deutekom JC, Datson NA. Digital droplet PCR for the absolute quantification of exon skipping induced by antisense oligonucleotides in (Pre-)clinical development for Duchenne muscular dystrophy. *PLoS One* 2016;**11**:e0162467. https://doi.org/10.1371/journal.pone.0162467
31. Young J, Margaron Y, Fernandes M *et al.* MyoScreen, a high-throughput phenotypic screening platform enabling muscle drug discovery. *SLAS Discovery* 2018;**23**:790–806. https://doi.org/10.1177/2472555218761102
32. Committee for the Update of the Guide for the Care and Use of Laboratory Animals. *Guide for the Care and Use of Laboratory Animals*. 8th ed, Washington (DC), National Academy of Sciences. 2011.
33. Young CS, Mokhonova E, Quinonez M *et al.* Creation of a novel humanized dystrophic mouse model of Duchenne muscular dystrophy and application of a CRISPR/Cas9 gene editing therapy. *J Neuromuscul Dis* 2017;**4**:139–45. https://doi.org/10.3233/JND-170218
34. t Hoen PA, de Meijer EJ, Boer JM *et al.* Generation and characterization of transgenic mice with the full-length human DMD gene. *J Biol Chem* 2008;**283**:5899–907.
35. Burki U, Keane J, Blain A *et al.* Development and application of an ultrasensitive hybridization-based ELISA method for the determination of peptide-conjugated phosphorodiamidate morpholino oligonucleotides. *Nucleic Acid Ther* 2015;**25**:275–84. https://doi.org/10.1089/nat.2014.0528
36. Beekman C, Janson AA, Baghat A *et al.* Use of capillary western immunoassay (Wes) for quantification of dystrophin levels in skeletal muscle of healthy controls and individuals with Becker and Duchenne muscular dystrophy. *PLoS One* 2018;**13**:e0195850. https://doi.org/10.1371/journal.pone.0195850
37. Echigoya Y, Mouly V, Garcia L *et al.* *In silico* screening based on predictive algorithms as a design tool for exon skipping oligonucleotides in Duchenne muscular dystrophy. *PLoS One* 2015;**10**:e0120058. https://doi.org/10.1371/journal.pone.0120058
38. Bouge AL, Murauer E, Beyne E *et al.* Targeted RNA-seq profiling of splicing pattern in the DMD gene: exons are mostly constitutively spliced in human skeletal muscle. *Sci Rep* 2017;**7**:39094. https://doi.org/10.1038/srep39094
39. Anthony K, Arechavala-Gomeza V, Taylor LE *et al.* Dystrophin quantification: biological and translational research implications. *Neurology* 2014;**83**:2062–9. https://doi.org/10.1212/WNL.0000000000001025
40. Wang RT, Barthelemy F, Martin AS *et al.* DMD genotype correlations from the Duchenne Registry: endogenous exon skipping is a factor in prolonged ambulation for individuals with a defined mutation subtype. *Hum Mutat* 2018;**39**:1193–202. https://doi.org/10.1002/humu.23561
41. van den Bergen JC, Ginjaar HB, Niks EH *et al.* Prolonged ambulation in Duchenne patients with a mutation amenable to exon 44 skipping. *J Neuromusc Dis* 2014;**1**:91–4. https://doi.org/10.3233/JND-140002
42. Blake DJ, Martin-Rendon E. Intermediate filaments and the function of the dystrophin–protein complex. *Trends Cardiovasc Med* 2002;**12**:224–8. https://doi.org/10.1016/S1050-1738(02)00166-4
43. Gao QQ, McNally EM. The dystrophin complex: structure, function, and implications for therapy. *Compr Physiol* 2015;**5**:1223–39. https://doi.org/10.1002/cphy.c140048
44. Wilson DGS, Tinker A, Iskratsch T. The role of the dystrophin glycoprotein complex in muscle cell mechanotransduction. *Commun Biol* 2022;**5**:1022. https://doi.org/10.1038/s42003-022-03980-y
45. Zhang S, Qin D, Wu L *et al.* Genotype characterization and delayed loss of ambulation by glucocorticoids in a large cohort of patients with Duchenne muscular dystrophy. *Orphanet J Rare Dis* 2021;**16**:188. https://doi.org/10.1186/s13023-021-01837-x
46. Cuellar TL, Barnes D, Nelson C *et al.* Systematic evaluation of antibody-mediated siRNA delivery using an industrial platform of THIOMAB-siRNA conjugates. *Nucleic Acids Res* 2015;**43**:1189–203. https://doi.org/10.1093/nar/gku1362
47. Li B, Qing T, Zhu J *et al.* A comprehensive mouse transcriptomic BodyMap across 17 tissues by RNA-seq. *Sci Rep* 2017;**7**:4200. https://doi.org/10.1038/s41598-017-04520-z
48. Bulfield G, Siller WG, Wight PA *et al.* X chromosome-linked muscular dystrophy (mdx) in the mouse. *Proc Natl Acad Sci USA* 1984;**81**:1189–92. https://doi.org/10.1073/pnas.81.4.1189
49. Frazier KS. Antisense oligonucleotide therapies: the promise and the challenges from a toxicologic pathologist's perspective. *Toxicol Pathol* 2015;**43**:78–89. https://doi.org/10.1177/0192623314551840
50. Lenz B, Braendli-Baiocco A, Engelhardt J *et al.* Characterizing adversity of lysosomal accumulation in nonclinical toxicity studies: results from the 5th ESTP International Expert Workshop. *Toxicol Pathol* 2018;**46**:224–46. https://doi.org/10.1177/0192623317749452
51. Birnkrant DJ, Ararat E, Mhanna MJ. Cardiac phenotype determines survival in Duchenne muscular dystrophy. *Pediatr Pulmonol* 2016;**51**:70–6. https://doi.org/10.1002/ppul.23215
52. Cheeran D, Khan S, Khera R *et al.* Predictors of death in adults with Duchenne muscular dystrophy-associated cardiomyopathy. *J Am Heart Assoc* 2017;**6**:e006340. https://doi.org/10.1161/JAHA.117.006340
53. Desjardins CA, Yao M, Hall J *et al.* Enhanced exon skipping and prolonged dystrophin restoration achieved by TfR1-targeted delivery of antisense oligonucleotide using FORCE conjugation in mdx mice. *Nucleic Acids Res* 2022;**50**:11401–14. https://doi.org/10.1093/nar/gkac641
54. Gan L, Wu LCL, Wood JA *et al.* A cell-penetrating peptide enhances delivery and efficacy of phosphorodiamidate morpholino

oligomers in mdx mice. *Mol Ther Nucleic Acids* 2022;**30**:17–27. https://doi.org/10.1016/j.omtn.2022.08.019
55. Sugo T, Terada M, Oikawa T *et al.* Development of antibody-siRNA conjugate targeted to cardiac and skeletal muscles. *J Control Release* 2016;**237**:1–13. https://doi.org/10.1016/j.jconrel.2016.06.036
56. Hanson B, Wood MJA, Roberts TC. Molecular correction of Duchenne muscular dystrophy by splice modulation and gene editing. *RNA Biol* 2021;**18**:1048–62. https://doi.org/10.1080/15476286.2021.1874161
57. Echigoya Y, Lim KRQ, Trieu N *et al.* Quantitative antisense screening and optimization for Exon 51 skipping in Duchenne muscular dystrophy. *Mol Ther* 2017;**25**:2561–72. https://doi.org/10.1016/j.ymthe.2017.07.014
58. Mukashyaka MC, Wu CL, Ha K *et al.* Pharmacokinetic/pharmacodynamic modeling of a cell-penetrating peptide phosphorodiamidate morpholino oligomer in mdx mice. *Pharm Res* 2021;**38**:1731–45. https://doi.org/10.1007/s11095-021-03118-5

Received: August 7, 2024. **Revised:** March 5, 2025. **Editorial Decision:** March 6, 2025. **Accepted:** March 18, 2025